

Vacuum joints of dispersion-strengthened copper and its applications in synchrotron radiation front end

Yong-Jun Li^{1,2} · Song Xue¹ · Min Zhang¹ ·
Dan-Dan Jia¹ · Dong-Bai Dou³ · Yu Gao³

Received: 12 August 2015 / Revised: 10 October 2015 / Accepted: 9 November 2015 / Published online: 12 October 2016
© Shanghai Institute of Applied Physics, Chinese Academy of Sciences, Chinese Nuclear Society, Science Press China and Springer Science+Business Media Singapore 2016

Abstract Masks are critical elements of synchrotron radiation front end that are exposed to high temperature and stress. The absorber material is typically comprised of dispersion-strengthened copper, which can retain high performance at elevated temperature. Joining processes under vacuum, including brazing and electron beam welding, are novel approaches for prolonging the absorber and for reducing power densities. The mechanical properties of brazed joints and electron beam welded joints of dispersion-strengthened copper workpieces are evaluated by tensile testing at 20, 100, and 200 °C. The testing results indicate that the tensile strength and elongation of both vacuum joints decrease with increasing temperature. Compared to brazed joints, electron beam welded joints have higher tensile strength, better ductility, and more stable performance. A novel welded mask with a total length of 600 mm is presented and shown to be practical for use in the highest heat load front end in the Shanghai synchrotron radiation facility phase-II beamline project.

Keywords Dispersion-strengthened copper · Brazing · Electron beam welding · Synchrotron radiation · Front end

✉ Yong-Jun Li
liyongjun@sinap.ac.cn

✉ Song Xue
xuesong@sinap.ac.cn

¹ Shanghai Institute of Applied Physics, Chinese Academy of Sciences, ZhangJiang, Shanghai 201204, China

² University of Chinese Academy of Sciences, Beijing 100049, China

³ SKY Technology Development Co., Ltd, Chinese Academy of Sciences, Shenyang 110179, China

1 Introduction

The Shanghai synchrotron radiation facility (SSRF) is an advanced third generation synchrotron light source with a 3.5-GeV electron storage ring and a designed beam current of 300 mA [1, 2]. Insertion devices, including undulators and wigglers, are always employed to generate high-quality synchrotron radiation. The power of an insertion device is up to several tens of kilowatts, and its peak power density can reach about 100 kW/mrad². The front end, which is an ultrahigh vacuum system following the electron storage ring, is primarily designed to handle the high heat load from the bending magnets or insertion devices. Masks are directly responsible for beam collimation and to protect the system from mis-steered beams, and are therefore critical elements of the front end that are directly exposed to high temperature and stress [3–5]. The absorbers of masks are generally comprised of dispersion-strengthened copper (DSC) at the SSRF, in addition to many other synchrotron radiation facilities, such as SPring-8, whose power and peak power density in the BL08 W beamline front end are 24.4 kW and 191 kW/mrad², respectively. Joining processes conducted under vacuum, including brazing and electron beam welding (EBW), are novel approaches for prolonging the life of the absorber and for reducing power densities.

DSC has been developed in recent years as an engineering material with excellent thermal conductivity, strength retention, and microstructural stability at elevated temperatures, and is widely applied in fields such as aerospace, electronics, mechanics, and synchrotron radiation [6–9]. The mechanical properties of DSC have been extensively studied [10–13]. In addition, the performance

Table 1 Physical properties of GlidCop AL-15 and oxygen-free high-conductivity copper (OFHC) at 20 °C

Physical properties	GlidCop AL-15	OFHC
Melting point (°C)	1083	1083
Density (g/cm ³)	8.9	8.9
Coefficient of thermal expansion (m/(m °C))	16.6	17.7
Thermal conductivity (W/(mm °C))	0.365	0.391
Young's modulus (GPa)	130	115
Poisson's ratio	0.326	0.323
Softening point (°C)	800	150

of brazed joints formed between DSC and other alloys have also been studied [14–17].

A DSC material, denoted as GlidCop AL-15 obtained from North American Hoganas High Alloys, is utilized in the SSRF phase-I front end, and was therefore selected in the present study to fabricate joint samples by means of vacuum brazing and vacuum EBW for tensile testing to meet the project requirements for the front end of the SSRF phase-II beamline project. The mechanical properties of the vacuum joint samples were evaluated by tensile testing at 20, 100, and 200 °C. A novel welded design for a high heat load mask is also presented, and the equivalent stress and strain on the EBW joint of the mask are much lower than the tensile testing results of EBW joints, which provide important guidance for its practical application.

2 Experimental procedures

2.1 Materials and procedures

GlidCop AL-15 is a type of Al₂O₃ DSC that is comprised of a pure copper matrix with a small amount (0.13–0.17 wt%) of extremely fine particles of Al₂O₃ (3–12 nm in diameter) dispersed throughout the matrix. The tensile strengths and elongations of this material at 20, 100, and 200 °C are, respectively, 420, 380, and 330 MPa and 27, 25, and 21 %. Table 1 lists the physical properties of GlidCop AL-15 and oxygen-free high-conductivity copper (OFHC) at 20 °C [18].

Vacuum brazing is commonly employed in vacuum systems owing to benefits such as small welding deformation and smooth joints [19]. A silver-based filler metal comprised of 74 % Ag and 26 % Cu was employed to join two GlidCop AL-15 workpieces using an L2116 double station furnace. The brazing was conducted at a heating rate of 10 °C/min and a brazing temperature of 800 °C with a holding time of 30 min followed by cooling in the furnace.

EBW is a fusion welding process conducted under vacuum, and provides high energy density, low heat input, and a rapid cooling rate [19, 20]. A WG-DZW-C electron

beam welder was employed for joining two GlidCop AL-15 workpieces at a pressure of 10⁻² Pa. A 60-kV voltage and a 50-mA beam current were precisely controlled to produce a beam of high-velocity electrons, resulting in a welding speed of 20 mm/s.

After welding, the tensile samples were machined according to GB/T 2651-2008 specifications (ISO 4136: 2001, IDT), as shown in Fig. 1. Tensile tests at room temperature were conducted using a DDL300 electronic universal testing machine based on GB/T 228.1-2010 specifications (ISO 6892-1: 2009, MOD), and a CSS-1120 electronic universal testing machine was employed for testing at elevated temperatures adopting GB/T 4338-2006 specifications (ISO 783: 1999, MOD).

2.2 Testing results on brazed joints

A total of 15 brazed joint tensile samples were separated into three groups randomly, and the mechanical properties at the three different temperatures were obtained. The results are listed in Table 2, where A is the elongation after fracture, R_m is the tensile strength, \bar{R} is the mean of R_m , and $R_s = \sqrt{\sum_{i=1}^5 (R_i - \bar{R})^2 / 4}$ ($i = 1-5$), is the standard deviation of R_m obtained by the Bessel formula. The fracture surfaces of all samples coincided with the joints.

As is shown in Table 2, none of the brazed joints underwent a yielding process, demonstrating that the brazed joints have very poor ductility. From the \bar{R} values, we see that the tensile strength decreased with increasing

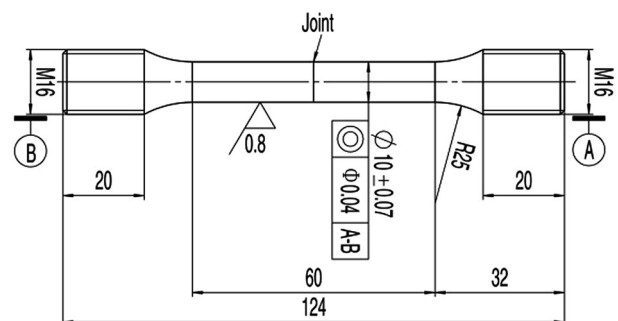


Fig. 1 Schematic of the machined tensile sample (unit: mm)

Table 2 Mechanical properties of the brazed joint samples

Test temperature (°C)	A (%)	R_m (MPa)							
		R_1	R_2	R_3	R_4	R_5	\bar{R}	R_s	
20	0	154	216	214	245	248	215	37.7	
100	0	120	181	173	235	224	187	45.8	
200	0	177	150	126	200	197	170	31.6	

temperature. Meanwhile, the tensile strength exhibits considerable variation at a given temperature with a maximum difference between sample values of 115 MPa and a maximum R_s of 45.8 MPa for samples tested at 100 °C, indicating that the brazed joints have low stability, and are not recommended for applications requiring high strength.

2.3 Testing results on EBW joints

As was conducted for brazed joints in Subsection 2.2, the mechanical properties of 15 EBW tensile samples were evaluated at the three different temperatures. The elongation and tensile strength results are listed in Tables 3 and 4, respectively, where \bar{A} is the mean of the elongation, and A_s is the standard deviation of A. The fracture surfaces of all samples also coincided with the joints.

All EBW joints underwent yielding processes with good consistency, demonstrating that EBW joints have some ductility. The tensile strength decreased with increasing temperature. Meanwhile, the tensile strength varies little at a given temperature with a maximum difference between values of 17 MPa and a maximum R_s of 6.4 MPa for samples tested at 100 °C, indicating that the EBW joints have high stability.

Table 3 Elongation of EBW joint samples

Test temperature (°C)	A (%)						
	A_6	A_7	A_8	A_9	A_{10}	\bar{A}	A_s
20	8.7	8.9	7.9	5.6	5.4	7.3	1.7
100	6.0	6.2	8.0	8.0	5.8	6.8	1.1
200	6.1	5.6	5.3	6.2	4.8	5.6	0.6

Table 4 Tensile strength of EBW joint samples

Test temperature (°C)	R_m (MPa)						
	R_6	R_7	R_8	R_9	R_{10}	\bar{R}	R_s
20	244	239	241	242	235	240	3.2
100	208	215	198	213	206	208	6.4
200	179	179	176	179	173	177	2.8

2.4 Vacuum joints versus GlidCop AL-15

The vacuum joint samples exhibited diminished mechanical properties relative to those of the GlidCop AL-15 base metal, as shown in Fig. 2. The tensile strength of brazed joints is only half that of the base metal and about 55 % for EBW joints. While the elongation of brazed joints approaches 0, the elongation of EBW joints is approximately 27 % that of GlidCop AL-15. The trends by which the mechanical properties of both joints change with changing temperature are consistent with the trend of the base metal.

3 Applications

A superconducting wiggler, serving as the source for the ultra-hard X-ray applications beamline at the SSRF, has an intensive power of over 43.3 kW and a peak power density of 45 W/mrad². Overlapping the radiation from upstream and downstream bending magnets, the total power will reach 44.7 kW, which results in the highest heat load for an SSRF phase-II beamline front end. Three fixed masks, whose absorbers are comprised of GlidCop AL-15, are

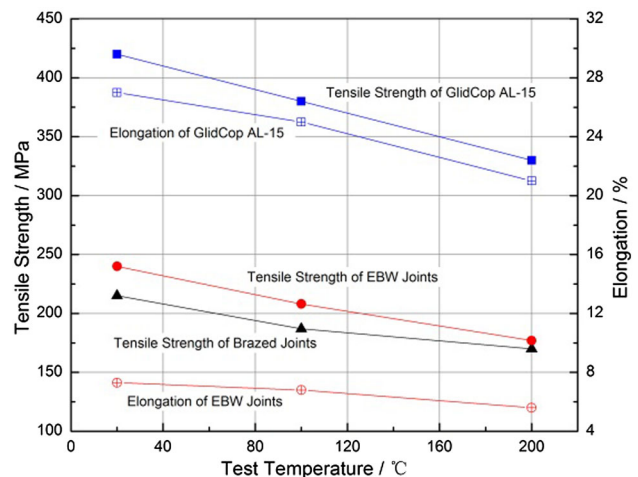
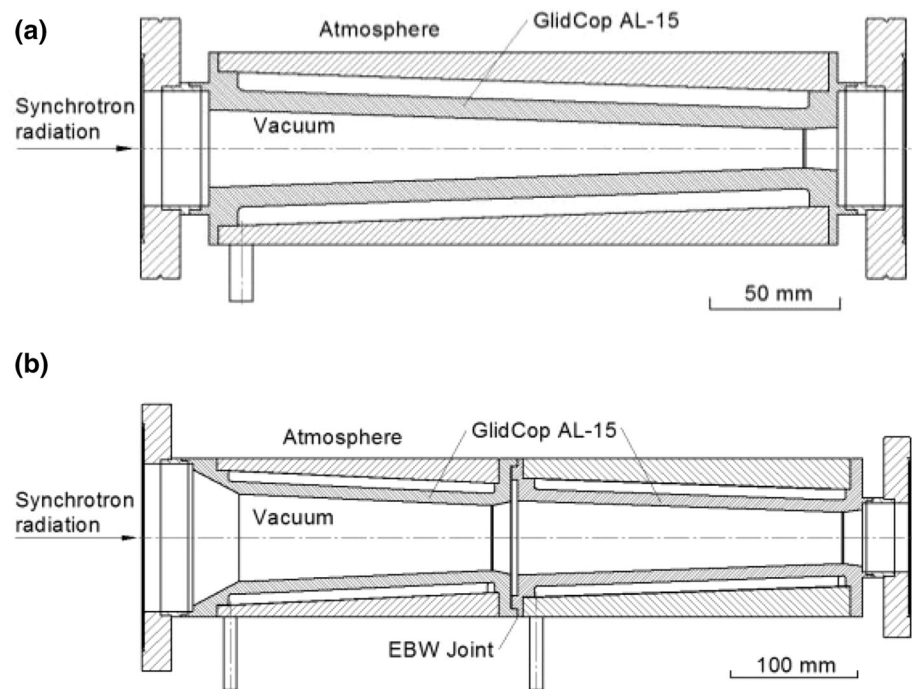


Fig. 2 Mechanical properties of vacuum joints versus the GlidCop AL-15 base metal

Fig. 3 Cross sections of a standard mask (a), and a welded mask (b)



located in sequence to handle this radiation. Figure 3a presents a cross section of a standard mask employed in an SSRF phase-I front end, which is comprised of a single absorber with a total length of about 300 mm. Figure 3b presents a cross section of a novel mask comprised of two sub-absorbers welded to each other by EBW, and a total length of about 600 mm. Ultrahigh vacuum exists inside all masks with ambient atmosphere outside.

Finite element analysis of the mask illustrated in Fig. 3b was conducted by ANSYS [20], which indicated that the highest temperature on the joint is 32.5 °C, and the maximum equivalent stress and strain are, respectively, 12.9 MPa and 0.118 %. While the tensile strength and elongation of an EBW joint at 32.5 °C can be determined to be 230.9 MPa and 1.6 %, respectively, by the interpolation method based on the testing results for EBW joint, these results lie far beyond the simulated stress and strain by ANSYS on the joint.

4 Conclusion

The mechanical properties of brazed joints and EBW joints formed from GlidCop AL-15 workpieces, which is a standard material utilized in the SSRF front end, were evaluated by tensile tests conducted at 20, 100, and 200 °C. The testing results showed that in comparison with the base metal, the tensile strength of both vacuum joints was reduced by nearly half and the elongation

reduced by 73 % or more. Compared to brazed joints, EBW joints demonstrated higher tensile strength, better ductility, and more stable performance. In practical engineering applications, vacuum joints are subjected to low stress and strain when not directly in the path of high power radiation. Therefore, EBW joints entirely satisfy the practical requirements. The brazed joints would be applicable in the front end as well only if welding parameters improved the ductility and stability of the resulting joints.

References

1. M.H. Jiang, X. Yang, H.J. Xu et al., Shanghai synchrotron radiation facility. *Chin. Sci. Bull.* **54**, 4171–4181 (2009). doi:10.1007/s11434-009-0689-y
2. Z.T. Zhao, L.X. Yin, Y.B. Leng, et al., Performance optimization and upgrade of the SSRF storage ring [C]. The 4th International Particle Accelerator Conference (IPAC2013), Shanghai, China, pp. 178–180 (2013)
3. D.M. Shu, M. Ramanathan, Design studies of the APS canted undulator beamline front ends. *Rev. Sci. Instrum.* **73**, 1580–1582 (2002). doi:10.1063/1.1435817
4. Y. Sakurai, M. Oura, S. Takahashi et al., Present status and performance of SPring-8 front ends. *J. Synchrotron Radiat.* **18**, 1195–1198 (1998). doi:10.1107/S0909049598002088
5. J.F. Jin, H.B. Chen, W.L. Xiao et al., Heat transfer analysis of the bent cooling channels in SSRF light-blocked components. *Nucl. Sci. Tech.* **23**, 321–327 (2012)
6. A. Nadkarni, E. Klar, W. Shafer, A new dispersion-strengthened copper. *Met. Eng. Q* **16**, 10–15 (1976)

7. M.X. Li, Z.M. Guo, Q.T. Zhao, Progress in and applications of copper-based alloys. *Powder Metall. Ind.* **18**, 36–40 (2008). doi:[10.3969/j.issn.1006-6543.2008.01.009](https://doi.org/10.3969/j.issn.1006-6543.2008.01.009)
8. T. Srivatsan, N. Narendra, J. Troxell, Tensile deformation and fracture behavior of an oxide dispersion strengthened copper alloy. *Mater. Des.* **21**, 191–198 (2000). doi:[10.1016/S0261-3069\(99\)00096-5](https://doi.org/10.1016/S0261-3069(99)00096-5)
9. J.Y. Chen, M.P. Wang, Progress in research on high-strength high-conductivity and high-heat resistance dispersion strengthened copper alloy. *Mater. Rev.* **18**, 38–42 (2004). doi:[10.3321/j.issn:1005-023X.2004.02.011](https://doi.org/10.3321/j.issn:1005-023X.2004.02.011)
10. T. Sunao, S. Mutsumi, M. Tetsuro et al., Fatigue life prediction for high-heat-load components made of Glidcop by elastic-plastic analysis. *J. Synchrotron Radiat.* **15**, 144–150 (2008). doi:[10.1107/S090904950706565X](https://doi.org/10.1107/S090904950706565X)
11. A. Meslet, M. Aldo, R. Woods et al., Influence of heat treatment on tensile response of an oxide dispersion strengthened copper. *J. Alloys.Comp.* **290**, 290–297 (1999). doi:[10.1016/S0925-8388\(99\)00227-3](https://doi.org/10.1016/S0925-8388(99)00227-3)
12. Z. Xiang, Z. Li, Q. Lei et al., High temperature mechanical behavior of alumina dispersion strengthened copper alloy with high content of alumina. *T. Nonferr. Metal.Soc.* **25**, 444–450 (2015). doi:[10.1016/S1003-6326\(15\)63622-6](https://doi.org/10.1016/S1003-6326(15)63622-6)
13. M. Avettand-Fènoëla, A. Simarb, R. Shabadia, Characterization of oxide dispersion strengthened copper based materials developed by friction stir processing. *Mater. Des.* **60**, 343–357 (2014). doi:[10.1016/j.matdes.2014.04.012](https://doi.org/10.1016/j.matdes.2014.04.012)
14. K. Zou, Study on vacuum brazing of Al₂O₃ dispersion-strengthened copper and CuCrZr alloy. Thesis, JiangSu University of Science and Technology, 2010
15. S. Chen, B. Chin, Low activation braze joint of dispersion-strengthened copper. *J. Nucl. Mater.* **225**, 132–136 (1995). doi:[10.1016/0022-3115\(94\)00524-9](https://doi.org/10.1016/0022-3115(94)00524-9)
16. H. Nishi, K. Kikuchi, Influence of brazing conditions on the strength of brazed joints of alumina dispersion-strengthened copper to 316 stainless steel. *J. Nucl. Mater.* **258–263**, 281–288 (1998). doi:[10.1016/S0022-3115\(98\)00230-X](https://doi.org/10.1016/S0022-3115(98)00230-X)
17. H. Nishi, T. Araki, M. Eto, Diffusion bonding of alumina dispersion-strengthened copper to 316 stainless steel with interlayer metals. *Fusion Eng. Des.* **39–40**, 505–511 (1998). doi:[10.1016/S0920-3796\(98\)00233-6](https://doi.org/10.1016/S0920-3796(98)00233-6)
18. North American Hogenas High Alloys home page. <http://www.hoganas.com/NAH>
19. L. Zeng, *Modern welding handbook* (Shanghai Science and Technology Press, Shanghai, 1993)
20. Z.H. Liu, X.F. Lei, B. Zhao et al., The study on local vacuum electron beam welding for aluminum alloy. *Nucl. Tech.* **25**, 755–757 (2002). doi:[10.3321/j.issn:0253-3219.2002.09.017](https://doi.org/10.3321/j.issn:0253-3219.2002.09.017)
21. Z.M. Xu, X.K. Feng, N.X. Wang et al., Thermal analysis of the first canted-undulator front end components at SSRF. *Nucl. Instrum. Methods A* **774**, 94–102 (2015). doi:[10.1016/j.nima.2014.11.082](https://doi.org/10.1016/j.nima.2014.11.082)